BBA - Bioenergetics 1867 (2026) 149581

Contents lists available at ScienceDirect

BBA - Bioenergetics

journal homepage: www.elsevier.com/locate/bbabio

Quantitative decomposition of non-photochemical quenching in *Physcomitrium patens* highlights synergistic roles of LhcSR and zeaxanthin

Cleo Bagchus [a], Lennart A.I. Ramakers [a], Dana Verhoeven [a], Claudia Beraldo [b], Alessandro Alboresi [b], Tomas Morosinotto [b], Herbert van Amerongen [a], Emilie Wientjes [a,*]

[a] *Laboratory of Biophysics, Wageningen University 6708, WE, Wageningen, the Netherlands*
[b] *Department of Biology, University of Padova, Via Ugo Bassi 58B, Padova, 35121, Italy*

ARTICLE INFO

Keywords:
PAM fluorescence
Light intensity
LHCSR
PsbS

ABSTRACT

Non-photochemical quenching (NPQ) is a collective term for photoprotective processes that safely dissipate excess light energy as heat. The moss *Physcomitrium patens* is an interesting species for the study of NPQ as it contains PsbS (indispensable for NPQ in vascular plants), LhcSR (indispensable for NPQ in green algae) and a xanthophyll cycle, which interconverts violaxanthin (Vx) and zeaxanthin (Zx) and is also imperative for NPQ. Here, we aimed to disentangle the individual contributions of PsbS, LhcSR and Zx to NPQ. NPQ induction and relaxation were measured for wild-type *P. patens* and thirteen mutants with altered NPQ at a wide range of light intensities. We applied a multivariate data analysis pipeline to find distinct kinetic components underlying NPQ, together with their contributions to NPQ. A slowly-rising component provides most NPQ, especially at higher light intensities. Another component contains a transient NPQ peak with a fast rise, providing quick protection, and requires the presence of either PsbS or LhcSR. Both components are enhanced by the combined presence of Zx and LhcSR. While PsbS-related NPQ is less dependent on Zx, in contrast to the situation in vascular plants, Vx to Zx conversion enhances LhcSR-related NPQ at all light intensities and within the first minute of illumination. The influence of Zx is thus broader than previously recognized, especially through its synergistic interaction with LhcSR.

1. Introduction

Photosynthesis converts light energy into chemical energy stored in the bonds of organic compounds. However, too much light is harmful for the photosynthetic apparatus. At higher light intensities, the rate of photon absorption exceeds the rate of photochemical quenching in the two photosystems. The excess energy increases the probability of triplet chlorophyll and singlet oxygen formation, which can cause photodamage [1–3]. To prevent such damage, photosynthetic organisms have evolved different photoprotective mechanisms [4]. An important mechanism is non-photochemical quenching (NPQ), a collective term for processes that are activated upon exposure to excess light and safely dissipate excess energy as heat [5–9]. Understanding the principles of NPQ is critical not only for elucidating fundamental photosynthetic mechanisms, but also for efforts to improve crop productivity under fluctuating light conditions [10–12].

There are multiple molecular mechanisms that contribute to NPQ in photosynthetic organisms. In vascular plants, the protein Photosystem II Subunit S (PsbS) is essential for NPQ formation [13,14]. PsbS is a member of the light-harvesting complex (LHC) superfamily but does not bind pigments [15,16]. This is in contrast to Light-Harvesting Complex Stress-Related (LhcSR) proteins, indispensable for NPQ in green algae [17], which do bind chlorophylls and xanthophylls [18]. LhcSR proteins are also members of the LHC superfamily [19]. Both PsbS [13] and LhcSR [18,20] are able to sense the low luminal pH induced by excess light, triggering the activation of NPQ. Low pH in the lumen also activates violaxanthin de-epoxidase (VDE) [21], which catalyzes the conversion of violaxanthin (Vx) to zeaxanthin (Zx) *via* antheraxanthin in the xanthophyll cycle [22,23]. Zx is a carotenoid that enhances NPQ and supports energy dissipation under excess light. Reconverting Zx back to Vx occurs in low-light conditions *via* zeaxanthin epoxidase (ZEP) [24]. Changes in the de-epoxidation state of the total pool of the xanthophyll pigments can be observed within minutes of light treatment [25,26]. Most Zx is reconverted to Vx within an hour after light stress [26,27]. In

* Corresponding author.
E-mail address: emilie.wientjes@wur.nl (E. Wientjes).

https://doi.org/10.1016/j.bbabio.2026.149581
Received 20 October 2025; Received in revised form 12 January 2026; Accepted 14 January 2026
Available online 15 January 2026

vascular plants, the full contribution of Zx to NPQ requires the presence of PsbS [28,29]. The quenching mechanism activated by PsbS, in functional interaction with Zx, is not known, but could involve for example lutein and trimeric LHCII [9,30,31]. In diatoms, the xanthophyll-dependent quenching requires the presence of Lhcx proteins [32–34], closely related to LhcSR proteins [35]. Most of our understanding of NPQ kinetics and its molecular basis comes from vascular plants, which lack LhcSR [36,37]. As a result, the interplay between LhcSR, PsbS and Zx remains unclear.

The moss *Physcomitrium patens*, the descendant of an evolutionary intermediate between green algae and vascular plants, is an interesting species to study NPQ, as both PsbS and LhcSR are constitutively expressed [36] and it has an active xanthophyll cycle [38]. In *P. patens*, both PsbS and LhcSR contribute independently to NPQ, with little evidence of mutual interaction. Of the two, LhcSR plays a larger role in providing photoprotection [36,39]. *P. patens* contains two LhcSR proteins (LhcSR1 and LhcSR2), with LhcSR1 accumulating to higher levels and generating most NPQ [36,39]. *P. patens* shows higher levels of NPQ than *Arabidopsis thaliana*, a model species for vascular plants [36]. Knock-out studies have shown that the presence of Zx is important for the formation NPQ in *P. patens* [40]. However, the interactions between LhcSR, PsbS and Zx were only probed at high light intensities.

In this study, we aim to disentangle the individual contributions of LhcSR, PsbS and Zx to NPQ in *P. patens* for a wide range of light intensities. Therefore, we employed a multivariate analysis pipeline that was previously developed for and applied to *A. thaliana* [41]. In *A. thaliana*, NPQ induction has been resolved into a limited number of kinetic components that have distinct contributions at different light intensities [29,41]. These components were correlated to important NPQ processes by studying mutants with altered NPQ and chemically-treated plants. A slowly-rising component was linked to the accumulation of Zx in presence of PsbS, while two faster components with a transient peak were associated with the rapid pH-dependent activation of PsbS [13,41]. Applying the analysis pipeline to *P. patens*, which expresses both PsbS and LhcSR, offers a unique opportunity to distinguish the individual roles and interactions of these proteins across a physiologically relevant light gradient.

We applied the multivariate data analysis pipeline [41] to *P. patens* to identify and quantify distinct kinetic components in NPQ induction and determine their association with PsbS, LhcSR, and Zx. NPQ induction and relaxation were measured with PAM fluorometry across a range of red actinic light intensities extending from below growth light to saturating light in wild-type *P. patens* and thirteen mutants affected in their NPQ. The resulting NPQ induction curves were analyzed with the multivariate analysis pipeline to resolve individual kinetic components and quantify their contributions to the total NPQ [41]. Analysis of the NPQ mutants enabled us to link individual kinetic components to PsbS, LhcSR and/or Zx. NPQ in *P. patens* can be accurately described with two kinetic components. A slowly-rising component is responsible for most NPQ, especially at higher light intensities. The contribution of this component is largely determined by the combination of Zx and LhcSR. The second component contains a transient peak and requires the presence of either PsbS or LhcSR, with LhcSR generating more NPQ. This component provides fast protection upon illumination changes. The LhcSR-related NPQ is heavily dependent on Vx to Zx conversion, at all light intensities and within a minute of illumination, while PsbS-related NPQ is less dependent on this conversion. Our results show that Vx to Zx conversion plays an extended role in NPQ, even at low light intensities, particularly in conjunction with LhcSR. These findings contribute to a more complete and quantitative understanding of photoprotection in early land plants.

2. Materials and methods

2.1. Plant material and growth conditions

P. patens Gransden wild type (WT) strain and mutants affected in their NPQ (*vde* KO [40], *vde psbs* KO [40], *vde lhcsr1 lhcsr2* KO ([40] from now on referred to as *vde lhcsr* KO), *psbs* KO [36], *lhcsr1* KO [36], *lhcsr2* KO[36], *lhcsr1 lhcsr2* KO (from now on referred to as *lhcsr* KO) [36], *psbs lhcsr1* KO [36], *psbs lhcsr2* KO [39], *psbs lhcsr1 lhcsr2* KO (from now on referred to as *psbs lhcsr* KO) [36], *zep* KO [42], *zep psbs* KO [43], *zep lhcsr1 lhcsr2* KO (from now on referred to as *zep lhcsr* KO; [43]) were included in this study (summarized in Supplementary Table 1). Protonemal tissue of *P. patens* was grown on minimal medium [44], supplemented with 0.5 g/L ammonium tartrate for both measurements and propagation. The plants were grown for 10–13 days at 50 μmol photons m^{-2} s^{-1} white light, with a 16 h light/8 h dark photoperiod and 60% relative humidity.

Chemical treatment was applied to inhibit certain processes important for NPQ. Protonemal tissue of *P. patens* was incubated with 5 mM D, L-dithiothreitol (DTT; inhibits among others the production of Zx) or 50 μM Nigericin (disrupts the pH difference across the thylakoid membrane) in 150 mM sorbitol, 10 mM 4-(2-hydroxyethyl)-1- piperazineethanesulfonic acid (HEPES; pH 7.5) buffer for at least 40 min in the dark at room temperature before measurements.

2.2. Pulse amplitude modulated (PAM) fluorometry

PAM fluorometry experiments were performed on a Mini-PAM-II (Walz), with a red actinic light source. Both red and blue light induce chloroplast movement in *P. patens* [45–47]. At higher light intensities, this light source could have initiated avoidance responses in chloroplasts. These avoidance responses decrease chlorophyll fluorescence, which increases the measured NPQ compared to the actual NPQ.

Before the measurements, plants were dark acclimated for at least 45 min. The measurement setup was controlled with a batch file in the WinControl-3.30 software supplied by Walz. Saturating pulses consisted of 6000 μmol photons m^{-2} s^{-1} for 800 ms. The $\frac{F_v}{F_m} = (F_m - F_o)/F_m$ was determined, followed by a period of darkness of 25 s. Subsequently, the red actinic light was switched on for 10 min at a light intensity between 15 μmol photons m^{-2} s^{-1} and 1150 μmol photons m^{-2} s^{-1}. The effect of the actinic light was probed with saturating pulses (F_m') to determine NPQ ($NPQ = (F_m - F'_m)/F'_m$). Saturating pulses were applied every ten seconds for the first two minutes, to capture the complex changes in the NPQ during this period, and every 30 s for the rest of the actinic light period. This regime of saturating pulses is likely slightly actinic in nature but did not affect the kinetics of NPQ induction in *A. thaliana* [41]. After the illumination period, far-red light was switched on for two seconds, at intensity setting twelve, to open the Photosystem II (PSII) reaction centers (RCs). This allowed us to determine the Fo' parameter, necessary for the calculation of the qP parameter ($qP = (F'_m - F')/(F'_m - F'_o)$), which is a proxy for the fraction of open PSII reaction centers. For the F_o' value, the minimum F value was determined in the thirty seconds after the far-red light was switched off. The mean of the ten F measurements surrounding this minimum value was taken as the F_o' measurement to account for measurement noise. This was followed by a nine-minute period of darkness, to allow for relaxation of NPQ, with saturating pulses every minute. Per light intensity, measurements were performed on at least three biological replicates.

2.3. Correction for the zep KO mutants

The *zep* KO mutants quench in the dark-adapted state, which lowers the apparent NPQ value and the dark-adapted $\frac{F_v}{F_m}$ value, measured with PAM fluorometry ([43]). The quenching in the dark can be identified by a decrease in the PSII fluorescence lifetime of the *zep* KOs in the dark-

adapted state when all RCs are closed (F_m). Based on the lifetime of WT in F_m, which does not quench in the dark-adapted state, a correction factor can be determined to correct for the lower F_m due to dark-adapted quenching [29]. This assumes the *zep* KO mutants would have the same dark-adapted F_m as WT plants in case they would not have had the dark-adapted quenching. This yields the following equation:

$$F_m^{No\ NPQ} = F_m^{Observed}\left[\frac{\tau_{F_m}^{No\ NPQ}}{\tau_{F_m}^{Observed}}\right]$$

where $F_m^{No\ NPQ}$ is the estimated value of the dark-adapted fluorescence yield with fully closed PSII RCs and no NPQ, $F_m^{Observed}$ is the measured value of the dark-adapted fluorescence yield with fully closed PSII RCs with long-term quenching (as in the *zep* KO mutants), $\tau_{F_m}^{No\ NPQ}$ is the theoretical value of the average dark-adapted fluorescence lifetime with fully closed PSII RCs and no NPQ (assumed to be the same as in WT plants) and $\tau_{F_m}^{Observed}$ is the measured value of the average dark-adapted fluorescence lifetime with fully closed PSII RCs with long-term quenching (as measured in the *zep* KO plants) [29].

To determine the average lifetimes necessary for the correction factor, the data from the streak-camera measurements on *P. patens* WT and *zep* KO's from Beraldo et al. [43] was used. These measurements were performed with PSII RCs that were closed by the application of DCMU. The MINI-PAM-II has a 700 nm cutoff for fluorescence. The streak-camera setup collects a wider range of the emission spectrum. To account for the cutoff in the MINI-PAM-II, the average lifetime was determined above 700 nm. This was achieved by determining the contributions of both the PSI and the PSII Decay-Associated Spectrum above 700 nm and multiplying these with their corresponding lifetimes. This average lifetime above 700 nm was determined for WT *P. patens*, the *zep* KO, the *zep psbs* KO and the *zep lhcsr* KO (Supplementary Fig. 1). These were then applied to correct the dark-adapted F_m of the *zep* KO mutants to account for the dark-adapted quenching (Supplementary Table 2). This allows us to determine whether the *zep* KO mutants reach similar steady-state NPQ levels as their respective counterparts that do no accumulate Zx.

2.4. Data analysis

Data analysis was performed with the multivariate analysis pipeline developed to deconvolute NPQ kinetics in vascular plants [41]. This pipeline resolves individual kinetic NPQ components with distinct contributions to the total NPQ from NPQ induction curves. Plants with an $\frac{F_v}{F_m}$ value of >0.65 were included in the data analysis pipeline, except for the *zep* KO [42], *zep psbs* [43], *zep lhcsr* KO [43] plants, where a cutoff value of 0.6 was applied, due to their quenching in the dark-adapted state ([43]).

Briefly, the pipeline first applies Principal Component Analysis (PCA) to extract components that vary strongly across the applied actinic light intensities (compared to the biological variance) (Supplementary Fig. 2) [48,49]. PCA can be performed with as many components as is necessary to account for most of the variance. A scree plot, which shows the percentage of the total explained variance *versus* the total number of components, helps to decide on the number of components. The elbow point, defined as the point with the maximum curvature, is a guideline for the number of components that are included [50]. Next, full harmonic phasor analysis (FH-phA) is applied to identify any additional components that do not vary as strongly with respect to the actinic light intensity changes (Supplementary Fig. 3) [51–54]. Each NPQ induction curve is transformed to the associated 2D phasor space, where the location of the point corresponds to the profile of the induction curve. Biological variation among the NPQ induction curves introduces scatter in this phasor data cloud. Based on the data cloud, the location of the point representing the average NPQ curve of the dataset and the location of the point representing the principle component(s) found with PCA, an extra component is located using Euclidian geometry [53,54]. The spread induced by biological variation among the NPQ induction curves reduces the precision with which the underlying kinetic components can be geometrically resolved. The combination of these techniques gives an approximation of the contributions of the induction profiles to the total NPQ, for each induction curve included in the data set. The contributions of the induction profiles are used as input for Non-negative Matrix Factorization (NMF) to allow for deconvolution of the data into NPQ components with distinct normalized induction profiles and their contributions to the total induced NPQ [41,55]. As NMF is applied to data with biological variation, the certainty with which component shapes can be resolved is correspondingly limited. The contributions of the individual components to each of the NPQ induction curves in the data set are fitted with either a linear relationship or a Hill-function, dependent on which fit results in the smallest error.

3. Results

In this study, we aimed to disentangle the kinetic components underlying NPQ in the moss *P. patens*. We have measured NPQ induction and relaxation curves with PAM fluorometry at a range of light intensities for WT *P. patens* and thirteen mutants with altered NPQ. The induction curves were analyzed with a multivariate analysis pipeline, previously developed to disentangle NPQ components in *A. thaliana* [41]. Analysis of the mutants, as well as chemically-treated *P. patens* to inhibit certain aspects of NPQ, enabled assignment of the obtained kinetic components to specific underlying NPQ processes.

3.1. The shape of the NPQ induction curve changes across light intensities

NPQ induction and relaxation was measured in WT *P. patens* with different red actinic light intensities ranging from 15 μmol photons m^{-2} s^{-1} to 1150 μmol photons m^{-2} s^{-1} (Fig. 1). The shape of the NPQ induction curve changed across the different light intensities. At low light intensities (<125 μmol photons m^{-2} s^{-1}), a transient peak in NPQ occurred after approximately a minute of illumination and relaxed to a relatively steady level of NPQ within five minutes of illumination. This fast induction of NPQ is thus counteracted by other effects that diminish NPQ, such as the dissipation of the pH difference across the thylakoid membrane by the activation of the ATP synthase, linked to the activation of the Calvin-Benson-Bassham cycle. The action of K^+-efflux antiporters can also diminish NPQ (see discussion) [56]. At higher light intensities, a small transient peak can still be observed, but instead of decaying to a

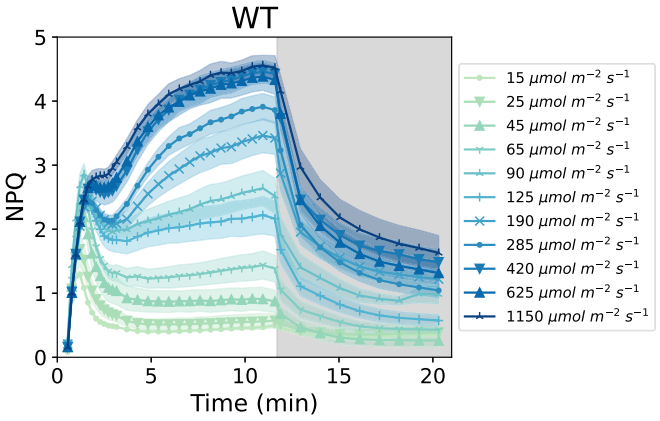

Fig. 1. WT *P. patens* NPQ induction and relaxation measured at different light intensities. White background indicates the illumination period, while a gray background indicates darkness. Markers indicate the location of saturating pulses, with the connecting line being an interpolation between these datapoints. Shading around the curves displays the standard error on the measurement. Light intensities are indicated in the legend. $n \geq 3$.

steady level, NPQ increased further to reach a steady state of NPQ at a level higher than the initial peak. The changes of the induction curve across light intensities indicate that there are distinct kinetic components underlying NPQ of which the contribution depends on the light intensity. A substantial part of the NPQ relaxed in the nine minutes of darkness following illumination.

3.2. Two distinct kinetic components can accurately describe NPQ induction in WT P. patens

Changes in the profile of the NPQ induction curves across a range of different light intensities can partly reveal the presence of different kinetic components underlying NPQ. The NPQ induction curves measured at different light intensities were analyzed using the multivariate data analysis pipeline [41]. The NPQ induction curves were ordered according to the approximate fraction of PSII reaction centers (RCs) closed at the end of the illumination period where a steady-state (ss) of NPQ is reached ($(1\text{-qP})_{ss}$). This parameter is used instead of the actual light intensity as the light intensity the moss receives can vary slightly. Nevertheless, $(1\text{-qP})_{ss}$ values correlated with the light intensity (Supplementary Fig. 4). Application of the $(1\text{-qP})_{ss}$ parameter also allows for better comparison of the effect of light intensities across different strains. However, equal $(1\text{-qP})_{ss}$ values do not necessarily correspond to equal luminal pH.

When fitting with two components, the data analysis pipeline results in two normalized, distinctly-shaped induction profiles (α and β) that underpin NPQ in WT *P. patens* (Fig. 2a). The α component rises slowly across the illumination period, reaching a steady state after approximately eight minutes. Fig. 2b shows the amount of NPQ corresponding to this component across the range of $(1\text{-qP})_{ss}$ values at the end of the illumination period. The amount of NPQ ranged from 0.0 at low light (most PSII RCs open) to 5.0 at high light (most PSII RCs closed). The second component (β) contains a transient peak, which decays to a steady state of NPQ within five minutes of illumination (Fig. 2a). The amount of NPQ generated by this component remained relatively constant across $(1\text{-qP})_{ss}$ values, starting at 1.8 for $(1\text{-qP})_{ss} = 0.2$ (low light intensity) and decreasing to 1.0 for $(1\text{-qP})_{ss} = 0.8$ (high light intensity) (Fig. 2c). The β component was responsible for most NPQ at low levels of RC closure, while at higher levels of RC closure, the α component generated more NPQ, explaining the complex shape changes observed in NPQ induction across light intensities (Fig. 1). Fig. 2d compares the reconstructed NPQ induction curves based on the analysis pipeline results (solid line) and the data (markers). The two distinct kinetic components and their contributions uncovered with the data analysis pipeline could indeed accurately describe the complex NPQ induction curves across different light intensities. The accurate description of the data is reflected by the high average adjusted r^2 value for the fit (0.96; Supplementary Fig. 5).

A fit with three components instead of two components only increased the average adjusted r^2 value of the NPQ reconstruction slightly from 0.96 to 0.98 (Supplementary Fig. 6). As the biological variation on the *P. patens* NPQ induction data is relatively large, it is difficult to identify the exact shape of the kinetic components. This leads to difficulty separating similarly-shaped kinetic components, such as the β and γ kinetic components in the three-component fit, which both contain a transient peak. In this study, we have therefore chosen to fit

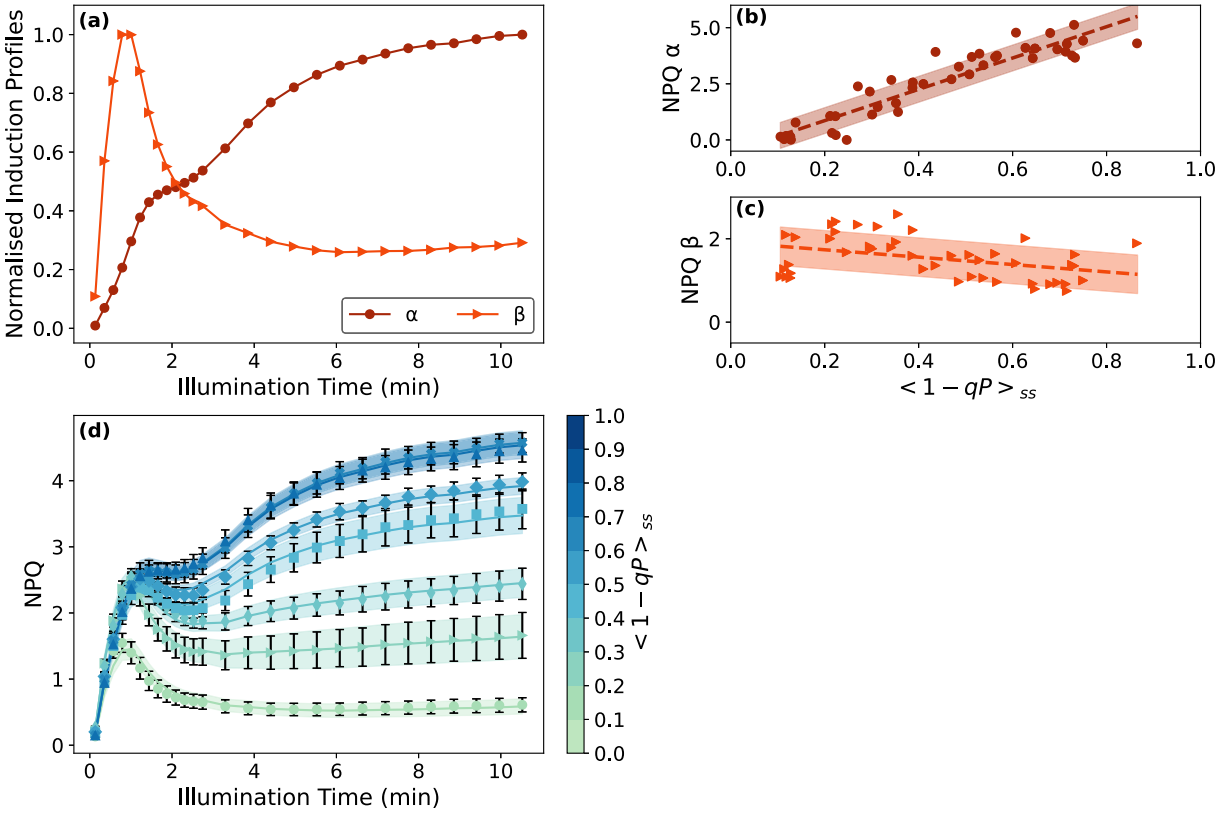

Fig. 2. Summary of the data analysis pipeline result for WT *P. patens*, compared to the original dataset. a. The normalized induction profiles of the two decomposed kinetic components (α and β) that underpin the NPQ induction curves. b/c. The amount of NPQ generated by the α (b) and β (c) decomposed kinetic components. The scatter points reflect the contribution of the specific component to the total NPQ in each of the NPQ induction curves in the data set. The contributions vary linearly across the $(1\text{-qP})_{ss}$ values. The fit is indicated by a dashed line and the standard deviation of the fit is shaded. d. Comparison of the NPQ reconstructed from the data analysis pipeline (solid line, where the shading indicates the standard error) and the original data (markers, with the standard error indicated by error bars). The data was binned according to its $(1\text{-qP})_{ss}$ value with a bin size of 0.1. The $(1\text{-qP})_{ss}$ bin of the data is indicated by the color bar. The NPQ constructed from the data analysis and the original data are only shown in the plot for bins with $n \geq 3$. $n \geq 3$ per light intensity for the original dataset (Fig. 1).

with two distinct kinetic components as these also accurately fit the data. This accurate fit of the NPQ induction in *P. patens* with only two components may seem surprising considering that PsbS, LhcSR and Zx all contribute to its NPQ [36,40]. However, more than one process might contribute to each component.

3.3. Role of PsbS, LhcSR and Zeaxanthin in shaping NPQ kinetics

To determine how these distinct NPQ components are related to the activity of PsbS, LhcSR and Zx, NPQ induction of the mutants was analyzed with the same analytical pipeline as for WT [41]. First, NPQ was induced in the *psbs lhcsr* KO [36] (Fig. 3a). This mutant line lacks both the PsbS and LhcSR proteins and generates far less NPQ than WT. Notably, the NPQ induction curves of this mutant lack the transient peak characteristic of the WT NPQ induction curve at lower light intensities (Fig. 3a). Most of the generated NPQ did not relax in nine minutes in the dark compared to WT, which indicates photodamage-related quenching due to the lower level of photoprotection (Supplementary Fig. 7a). The NPQ induction curves of the *psbs lhcsr* KO mutant were similar to induction curves of WT treated with nigericin (Supplementary Fig. 8a), which is a pH uncoupler [57]. PsbS and LhcSR are activated upon acidification of the thylakoid lumen and are therefore not active in nigericin-treated WT [13,20]. Acidification of the thylakoid lumen activates VDE as well [21], so the generation of Zx is also impaired in nigericin-treated WT. The similarity between the *psbs lhcsr* KO and the nigericin-treated WT suggests that Zx-dependent NPQ is also impaired in this mutant.

For the dataset of the *psbs lhcsr* KO a fit with two components in the data analysis pipeline (the same number as for WT) accurately described the data, with an average adjusted r^2 of 0.99 (Supplementary Fig. 7c). A slowly-rising NPQ component was present in the *psbs lhcsr* KO, similar to WT but with a slightly slower initial rise (Fig. 3c). This component generates much less NPQ compared to WT, with a maximum around one instead of five (Fig. 3b). WT development of the slowly-rising

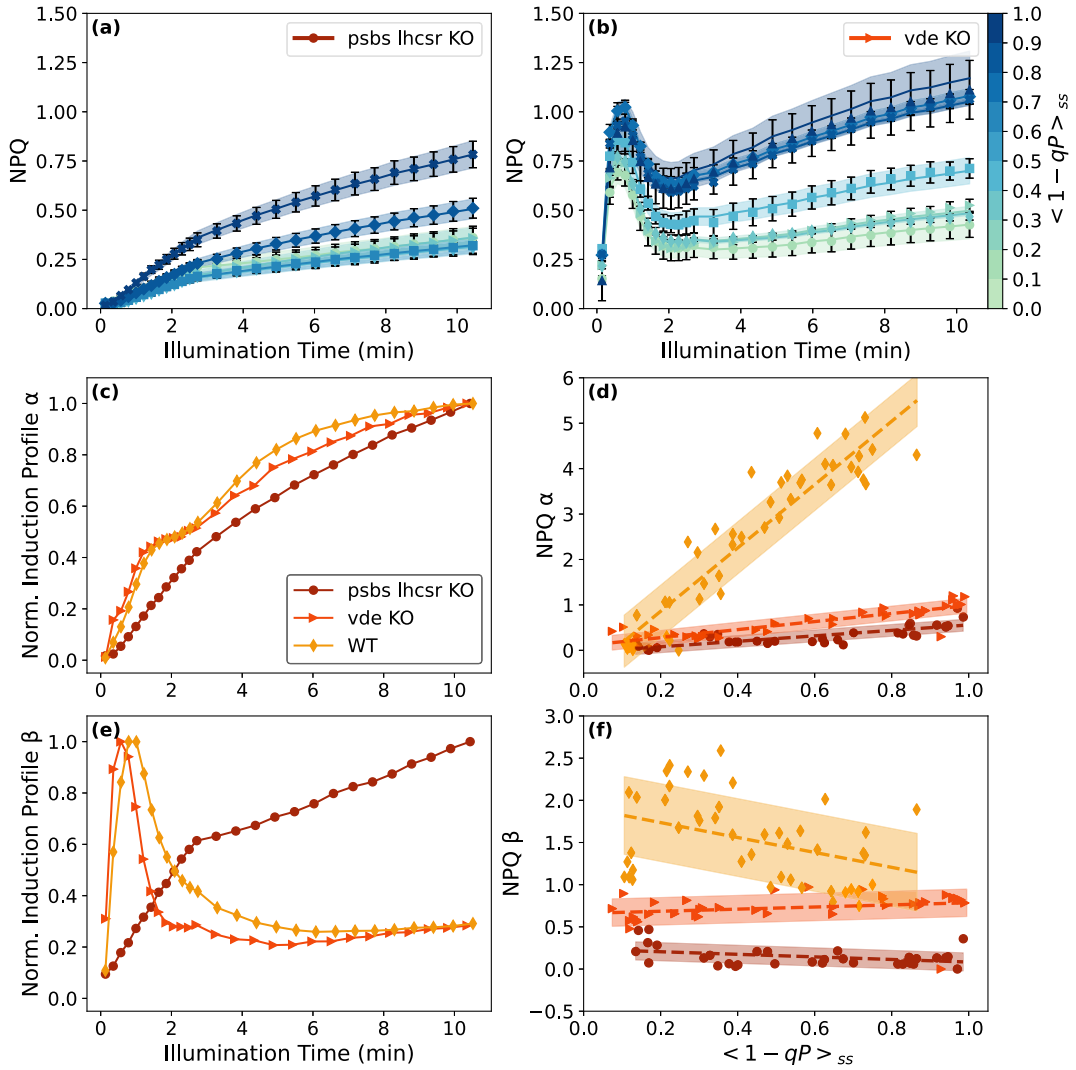

Fig. 3. Summary of the analysis pipeline result for psbs lhcsr KO and vde KO *P. patens*, compared to the original datasets. a/b. Comparison of the NPQ reconstructed from the data analysis pipeline (solid line, where the shading indicates the standard error) and the original data (markers, with the standard error indicated by error bars) for *psbs lhcsr KO* (a) and *vde KO* (b). The data was binned according to its $(1\text{-qP})_{ss}$ value with steps of 0.1. The color bar indicates the $(1\text{-qP})_{ss}$ bin of the data for both mutants. The NPQ constructed from the data analysis and the original data are only shown in the plot for bins with $n \geq 3$. c/e. The normalized induction profile of the α (c) and β (e) kinetic components that underpin the NPQ induction curves of the different mutants. Data from WT (Fig. 2a) is added for ease of comparison. d/f. The amount of NPQ generated by the α (d) and β (f) decomposed kinetic components for each mutant. The data from WT (Fig. 2b/c) is added for ease of comparison. The scatter points reflect the contribution of the specific component to the total NPQ in each of the NPQ induction curves in the data set. The contributions vary linearly across the $(1\text{-qP})_{ss}$ values. The fit is indicated by a dashed line and the standard deviation of the fit is shaded. $n \geq 3$ per light intensity for the original dataset (Supplementary Fig. 7).

component thus required the presence of PsbS and/or LhcSR. The second kinetic component, with a low contribution, had a completely different shape in the *psbs lhcsr* KO than in WT. In the mutant, the component lacked the transient peak and instead rose slowly over the entire illumination period. This suggests that during NPQ, quenching dependent on the presence of PsbS and/or LhcSR quickly rises and then relaxes to a steady state within a few minutes, potentially due to dissipation of the pH difference across the thylakoid membrane.

3.4. Zx enhances both components

Subsequently, NPQ was induced in the *vde* KO (unable to produce Zx from Vx; [40]) (Fig. 3). In contrast to the NPQ induction curves of the *psbs lhcsr* KO (Fig. 3a), the NPQ induction curves of the *vde* KO show a transient peak even at high levels of RC closure (Fig. 3b). The peak is reached approximately one minute after the start of the illumination and NPQ is lower compared to WT across the complete range of RC closure. This suggests Vx to Zx conversion influences NPQ production within a minute of illumination even at low light intensities. Like for the *psbs lhcsr* KO, a substantial part of the generated NPQ did not relax after the illumination period, which suggests photodamage-related quenching (Supplementary Fig. 7b). The NPQ induction in the *vde* KO indeed closely resembled NPQ induction in WT plants treated with DTT, which disrupts the xanthophyll cycle, preventing formation of Zx (Supplementary Fig. 8b) [58], suggesting that the lack of Zx is responsible for these changes.

A two-component fit of the NPQ induction curves of the *vde* KO in the data analysis pipeline resulted in an average adjusted r^2 of 0.93 (Supplementary Fig. 7d). The *vde* KO contained a slowly-rising component as well, almost identical in shape to the WT component (Fig. 3c). This component generates similar levels of NPQ as the *psbs lhcsr* KO and much less NPQ than WT (around one instead of five) (Fig. 3b). The contribution of the slowly-rising component at WT levels thus required Vx to Zx conversion and the presence of PsbS and/or LhcSR. In contrast to the

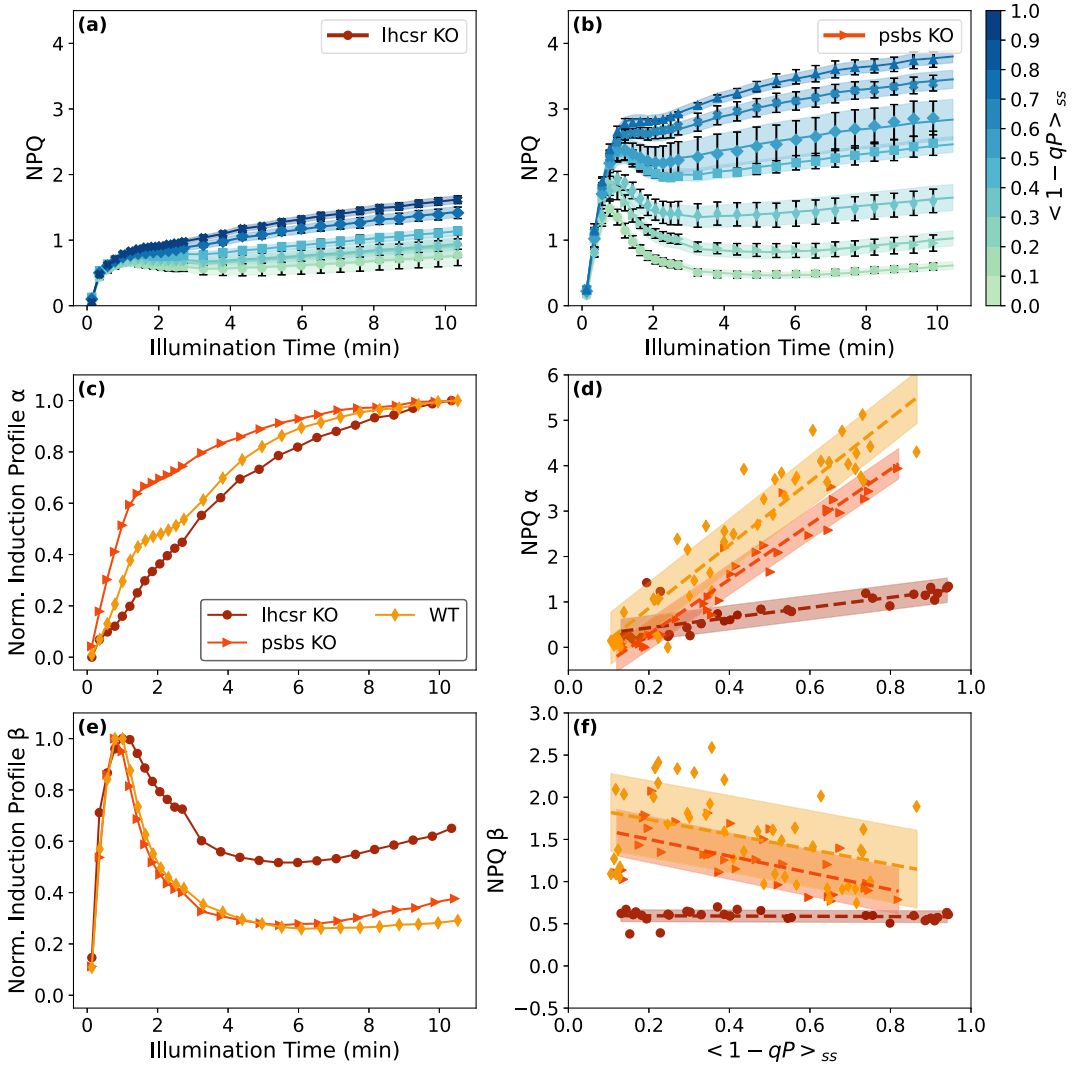

Fig. 4. Summary of the analysis pipeline result for the *lhcsr KO* and *psbs KO P. patens*, compared to the original datasets. a/b. Comparison of the NPQ reconstructed from the data analysis pipeline (solid line, where the shading indicates the standard error) and the original data (markers, with the standard error indicated by error bars) for *lhcsr KO* (a) and *psbs KO* (b). The data was binned according to its $(1\text{-qP})_{ss}$ value with steps of 0.1. The color bar indicates the $(1\text{-qP})_{ss}$ bin of the data for both mutants. The NPQ constructed from the data analysis and the original data are only shown in the plot for bins with $n \geq 3$. c/e. The normalized induction profile of the α (c) and β (e) kinetic components that underpin the NPQ induction curves of the different mutants. Data from WT (Fig. 2a) is added for ease of comparison. d/f. The amount of NPQ generated by the α (d) and β (f) kinetic components for the mutants. The data from WT (Fig. 2b) is added for ease of comparison. The scatter points reflect the contribution of the specific component to the total NPQ in each of the NPQ induction curves in the data set. The contributions vary linearly across the $(1\text{-qP})_{ss}$ values. The fit is indicated by a dashed line and the standard deviation of the fit is shaded. $n \geq 3$ per light intensity for the original dataset (Supplementary Fig. 9).

psbs lhcsr KO, the fastest induction profile of the *vde* KO was similar to the fastest profile in WT, where a transient peak in NPQ was formed due to the presence of PsbS/LhcSR. The contribution of this component was higher in WT than in the *vde* KO (around 1.8 instead of 0.9), indicating that the ability to form Zx enhances the contribution of this NPQ component as well, especially at lower light intensities. The conversion of Vx to Zx thus enhances both kinetic components.

3.5. Both LhcSR and PsbS generate NPQ quickly upon illumination, with LhcSR producing more NPQ

The presence of PsbS and/or LhcSR was required for the quick formation of NPQ upon illumination, as shown by the *psbs lhcsr* KO. The NPQ relaxes within four minutes at lower light intensities to form a transient peak. To determine how each of these proteins impacted NPQ, the induction curves of the *psbs* KO and the *lhcsr* KO mutants were measured at the same range of light intensities (Fig. 4). Compared to WT, a lack of LhcSR (both LhcSR1 and LhcSR2) decreases the NPQ substantially (approximately four-fold), while the lack of PsbS only slightly decreases the maximum level of NPQ. LhcSR thus provides a large contribution to NPQ formation. With only PsbS present, the prominence of the initial peak in NPQ is decreased compared to WT. There are no major changes in the shape of the NPQ induction curve between the *psbs* KO (that contains LhcSR) and the WT. Both the *lhcsr* KO and the *psbs* KO show relaxation of a substantial amount of NPQ in the nine minutes following illumination (Supplementary Fig. 9a/b).

To more precisely pinpoint the contributions of LhcSR and PsbS to NPQ, the NPQ induction curves were analyzed with the data analysis pipeline. Again, an accurate fit was reached with only two components (Supplementary Fig. 9c/d). Both mutants contained a slowly-rising component (Fig. 4c). At lower levels of RC closure $(1\text{-qP})_{ss}$ (<0.25), this component generates almost no NPQ for all mutants (Fig. 4d). With more RCs closed, there were distinct differences between the mutants. In the *psbs* KO, the slowly-rising component generated almost as much NPQ as in WT, demonstrating the importance of LhcSR. In the *lhcsr* KO, the contribution of the slowly-rising component was much lower and similar to the contribution in the *vde* KO. Analysis of NPQ induction in the *lhcsr* KO and the *vde* KO indicates that both the ability to form Zx and the presence of LhcSR are required for full development of NPQ by the slowly-rising component.

Both the *lhcsr* KO and the *psbs* KO contained a second component with a transient peak that quickly rises in time, suggesting that both PsbS and LhcSR are capable of inducing NPQ quickly upon illumination. In the *psbs* KO, this component generated similar levels of NPQ compared to WT, but the contribution to NPQ was much lower in the *lhcsr* KO. The other combinations of *psbs*, *lhcsr1* and *lhcsr2* KOs were analyzed as well and indicated that LhcSR1 is responsible for most of the NPQ, with only a minor role for LhcSR2 (Supplementary Fig. 10). The similarity in shape

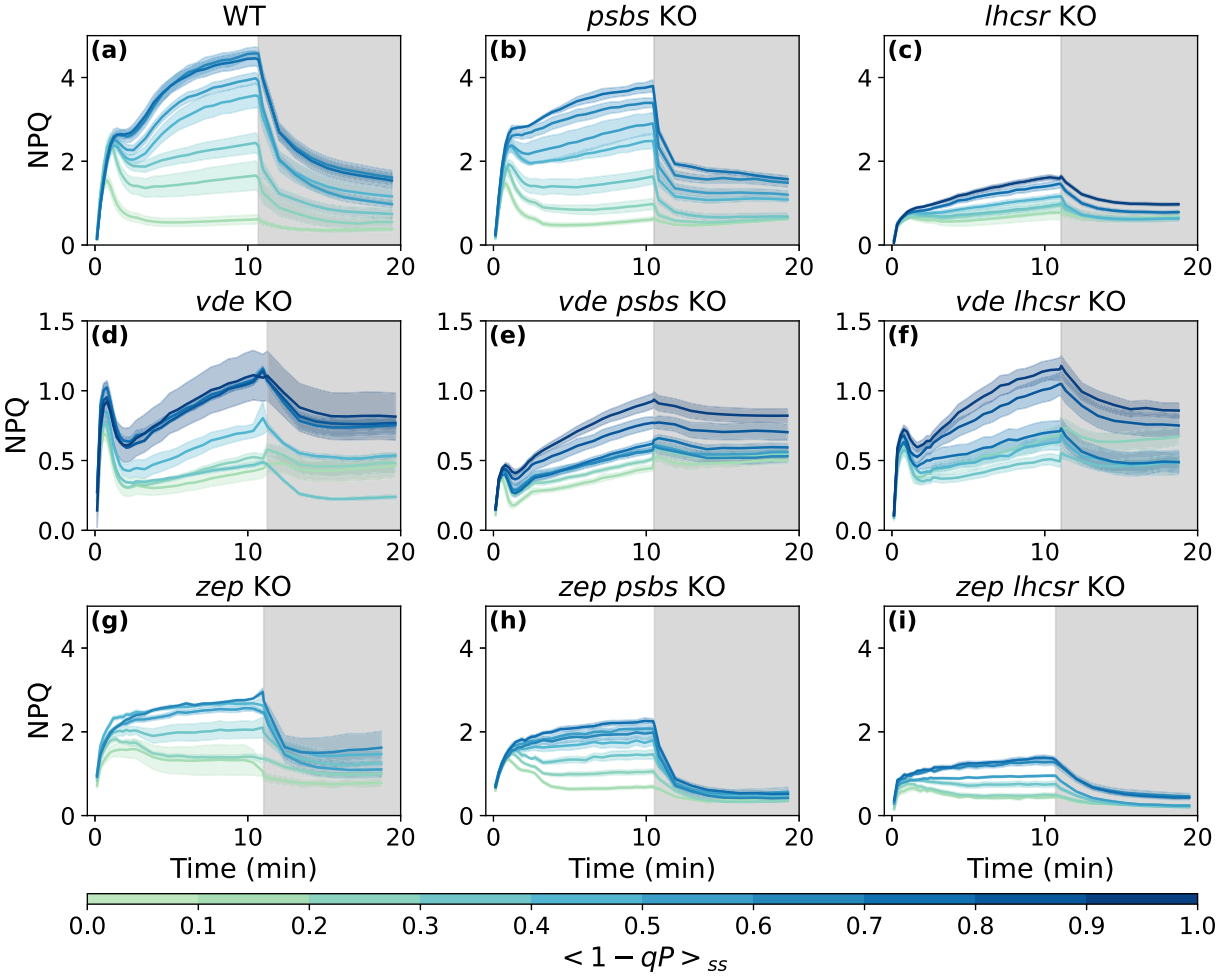

Fig. 5. NPQ induction and relaxation for NPQ mutants of *P. patens* measured at different light intensities. a. WT (data in Fig. 2c, added for ease of comparison). b. *psbs* KO (data in Fig. 4b, added for ease of comparison). c. *lhcsr* KO (data in Fig. 4a, added for ease of comparison). d. *vde* KO (data in Fig. 3b, added for ease of comparison). e. *vde psbs* KO. f. *vde lhcsr* KO. g. *zep* KO. h. *zep psbs* KO. i. *zep lhcsr* KO. White background indicates the illumination period, while a gray background indicates darkness. The data was binned according to its $(1\text{-qP})_{ss}$ value with steps of 0.1. The color bar below the graphs indicates the $(1\text{-qP})_{ss}$ bin of the data for all mutants. Only bins with $n \geq 3$ are shown in the plot. Shading displays the standard error on the measurement. n ≥ 3 per light intensity for the original datasets.

of the NPQ induction profiles for the *lhcsr* KO and the *psbs* KO clarify why the contributions of PsbS and LhcSR are difficult to separate in WT *P. patens*. Both PsbS and LhcSR are thus able to generate NPQ quickly upon illumination, although PsbS-related NPQ is lower.

3.6. Zx enhances quenching by LhcSR

WT-level generation of NPQ requires the combined presence of Zx and LhcSR, with less dependence on PsbS. To further explore this requirement, NPQ induction curves were measured for mutants with both altered Zx levels (either no presence of Zx or a constitutive presence of Zx) and a knock-out of LhcSR or PsbS (Fig. 5).

The *vde* KO mutants do not produce Zx and therefore generate less NPQ. As discussed above, the *vde* KO contains a clear transient peak in NPQ across the complete range of RC closure (Fig. 3b, Fig. 5d). The NPQ induction curves of both the *vde psbs* KO and the *vde lhcsr* KO mutants follows a similar trajectory as the *vde* KO, but with a lower initial peak of around 0.5 instead of 1 (Fig. 5e–f). Both the *vde psbs* KO and the *vde lhcsr* KO mutant exhibit a higher rise in NPQ after the initial peak than the *vde* KO. This subsequent rise in NPQ might have been caused by photodamage-related quenching, as suggested by the lack of NPQ relaxation in darkness. The *vde psbs* KO, containing only LhcSR, generates less NPQ than the *vde lhcsr* KO, containing only PsbS. This is surprising, as in *P. patens* able to convert Vx to Zx, LhcSR generates substantially more NPQ than PsbS (Fig. 4). The difference between the NPQ induction curves of the *psbs* KO mutant (containing LhcSR and Zx; Fig. 5b) and the *vde psbs* KO mutant (containing only LhcSR; Fig. 5e) started at the lowest levels of RC closure and was apparent within the first minute of illumination. This suggests a rapid effect of Vx to Zx conversion on the LhcSR-dependent NPQ even at low light intensities. The difference between the NPQ induction curves of the *lhcsr* KO mutant (containing PsbS and Zx; Fig. 5c) and the *vde lhcsr* KO mutant (containing only PsbS; Fig. 5f) is mostly in shape, with only a small increase in total NPQ (Supplementary Fig. 11 for the graphs shown on the same axis). The initial peak is broader in the *lhcsr* KO than in the *vde lhcsr* KO. The *lhcsr* KO treated with DTT to disrupt the xanthophyll cycle, preventing formation of Zx, also generated more NPQ compared to the DTT-treated *psbs* KO (Supplementary Fig. 12) [58]. This confirms that Zx formation is important for LhcSR-dependent quenching across different light intensities.

To better quantify the *vde* KO mutants, the NPQ induction curves of these mutants were analyzed with the data analysis pipeline (Supplementary Fig. 13). Two components were enough to reach an accurate fit (Supplementary Fig. 14 c/d). The shape of the two components was similar for all *vde* KOs. Comparison of the *vde lhcsr* KO and the *lhcsr* KO showed no enhancing effect of Vx to Zx conversion on the transient kinetic component and only a 0.3-fold increase for the slowly-rising kinetic component. This indicates that Zx only enhances PsbS-dependent quenching slightly. Between the *psbs* KO and the *vde psbs* KO, the enhancing effect of the Vx to Zx conversion on both components is clear with around an five-fold increase for the slowly-rising component and a four-fold increase for the transient component. This enhancing effect of Zx indicates the cooperativity between Zx and LhcSR. Overall, the enhancing effect of Zx suggests stronger cooperativity between Zx and LhcSR compared to Zx and PsbS.

3.7. Constitutive presence of Zx results in higher initial quenching

The interaction between Zx and PsbS and LhcSR was also investigated in *zep* KO mutants. While the *vde* KOs cannot produce Zx, the *zep* KOs have a constitutive presence of Zx, even in the dark-adapted state. Notably, these mutants reach lower levels of steady state NPQ compared to their respective mutants without constitutive accumulation of Zx (Fig. 5). This lower quenching could be due to quenching in the dark-adapted state, which is partly dependent on the presence of LhcSR, but not PsbS [43]. Indeed, the difference between the steady state NPQ levels is larger in the mutants that contain LhcSR compared to the mutant that does not contain LhcSR. This quenching in the dark-adapted state decreases the apparent/measured NPQ in these mutants as it decreases the dark-adapted F_m value. A correction for this lower dark-adapted F_m value in the *zep* KO mutants can be applied under the assumption that major PSII properties affecting variable fluorescence do not differ substantially between strains and that the observed difference in F_m values arises from varying levels of dark-adapted quenching. If this assumption holds true, the *zep* KO mutnats could reach WT F_m values without this dark-adapted quenching. Once we perform this correction [29], using data from [43], the corrected steady-state NPQ values in the *zep* KOs are more similar compared to their respective mutants lacking the *zep* KO (Supplementary Fig. 15). This suggests that the lower steady state NPQ is mostly due to the quenched dark-adapted state.

The *zep* KO mutant (Fig. 5g), uncorrected for the dark-adapted quenching, exhibits higher NPQ in the initial timepoint after illumination compared to the WT (Fig. 5a), most likely due to a pre-quenched state. The shape of the NPQ induction curve is somewhat different between the WT and the *zep* KO as well, with a less pronounced transient peak in the *zep* KO mutant. This higher initial quenching and this less pronounced transient peak is observed in the *zep psbs* KO (Fig. 5h) compared to the *zep lhcsr* KO (Fig. 5b) as well. These differences seem smaller when comparing the *zep lhscr* KO (Fig. 5i) and the *lhcsr* KO (Fig. 5c). This lack of difference suggests that LhcSR is impacted more by the accumulated Zx compared to PsbS.

To further explore the effect of a constitutive presence of Zx, the NPQ induction curves of the *zep* KO mutants were analyzed with the data analysis pipeline (Supplementary Fig. 16). An accurate fit was reached with two components for all mutants (Supplementary Fig. 17). The shape of the slowly-rising component was similar for the *zep* KO mutants and WT *P. patens* (Supplementary Fig. 16d). The transient kinetic component was elevated at the beginning of the illumination period in the *zep* KO mutants, but followed a similar trajectory afterwards. The contributions are smaller for the *zep* KO compared to WT, most likely due to the dark-adapted quenching which lowers the apparent NPQ. Both components contribute more at lower $(1\text{-qP})_{ss}$ values, potentially due to the pre-quenched state. These differences in contribution and shape of the kinetic components explain the changes observed in NPQ induction curves in the *zep* KO mutants.

4. Discussion

The coexistence of PsbS and LhcSR in *P. patens* offers an interesting model system for disentangling their respective contributions to NPQ and exploring their interactions. *P. patens* grows in moist, open soils along paths and in fields, as well as in seasonally wet areas [59] and as such can receive quite a high light intensity in its natural habitat, making efficient NPQ essential. During evolution, vascular plants have lost LhcSR and retained PsbS to provide NPQ [36,37]. Dissecting the contributions of PsbS and LhcSR to NPQ and their functional interactions with Zx may begin to provide insights into why vascular plants evolved to depend on PsbS rather than LhcSR.

While the effects of PsbS, LhcSR and Zx have been studied in *P. patens* before, this only occurred at higher light intensities ($>$ 800 μmol photons m^{-2} s^{-1}) [29,36,39,40,60,61]. These studies revealed that PsbS and LhcSR contribute independently to NPQ, with the LhcSR-dependent NPQ being larger and more reliant on Zx. NPQ has only been induced with a range of light intensities in WT *P. patens* [61], but not in any NPQ mutants. Studying NPQ induced at a range of light intensities can reveal interactions not visible at high light. The differences between NPQ induction curves at different light intensities can also partly reveal the kinetic components underlying NPQ, which can thus be isolated. We employed a multivariate data analysis pipeline, previously applied to *A. thaliana* [41], to elucidate distinct NPQ components in *P. patens*. We measured NPQ induction and relaxation curves of WT *P. patens* and thirteen mutants with altered NPQ. The resulting kinetic profiles were

used to assess how Zx, PsbS, and LhcSR individually and collectively shape the NPQ response across different light intensities.

NPQ induction in *P. patens* could be accurately described with just two kinetic components. The first component slowly rises to a steady state in about 10 min. The second kinetic component necessary to describe NPQ induction is characterized by a transient peak in NPQ that reaches its maximum after approximately one minute of illumination. Due to the biological variation in *P. patens,* small differences in shape of the components between mutants may not be significant.

4.1. The slowly-rising kinetic component

The slowly-rising component provides most of the NPQ at the steady state, especially at higher light intensities. A similar kinetic component was found when disentangling the NPQ induction in WT *A. thaliana* (which lacks LhcSR, but does contain PsbS), although with a lower contribution to NPQ [41]. As a slowly-rising component occurs in all the mutants measured in this study, it is likely that different processes cause a similar NPQ induction profile.

Both the WT and the *vde* KO have a slowly-rising component that is nearly identical in shape, but this component has a much lower contribution to NPQ in the *vde* KO (Fig. 3). This difference in contribution suggests that the ability to generate Zx is important to fully generate NPQ with the slowly-rising component. The kinetics of this component are indeed similar to the kinetics of Zx formation, as measured by absorbance changes between 505 and 565 nm [62] and changes in the de-epoxidation state of the total pool of the xanthophyll pigments [26,63]. It has been shown in *A. thaliana* that the de-epoxidation state of the xanthophyll cycle pool, so the concentration of Zx relative to the total xanthophyll pool, regulates NPQ, instead of the amount of produced Zx [64].

Interestingly, the kinetics of this slowly-rising component are similar for the WT and the *zep* KO, which has a constitutive presence of Zx (Supplementary Fig. 15). The contribution is slightly lower in the *zep* KO mutant (Supplementary Fig. 16), potentially due to its dark-adapted quenching [43]. This similarity in shape holds true as well in WT *A. thaliana* and the *npq2* mutant with a constitutive presence of Zx [29]. This similarity in the shape and contribution of the kinetic component between WT and the *zep* KO suggests that the production of Zx alone is not sufficient for the quenching *via* this component, but that an additional step or interaction partner is required. The lack of LhcSR lowers the contribution of this component (Fig. 4d). This suggests that an interaction with LhcSR is necessary for the formation of a quencher in this component. LhcSR is indeed able to bind Zx [18,40]. Without LhcSR present, there is a slight 0.3-fold enhancement of the slowly rising component if Zx is present, as indicated by a comparison of the *lhcsr* KO and the *vde lhcsr* KO (Supplementary Fig. 12). This slight increase suggests some functional interaction between PsbS and Zx. However, most of the quenching of this component is thus dependent on the presence of LhcSR. In summary, the slowly-rising NPQ component is strongly enhanced by the ability to form Zx and the presence of LhcSR.

A slowly-rising component was also present in mutants that lack LhcSR or VDE, although with a lower contribution to the total NPQ (Fig. 3). Processes not dependent on Vx to Zx conversion could therefore cause a limited amount of quenching that slowly rises across the illumination period as well. Due to the lower level of photoprotection, the chance of photodamage increases in the mutants without the ability to convert Vx to Zx. Photodamage-related quenching is expected to increase across the illumination period. Photodamage is slowly reversible and would not relax in the nine minutes of darkness following illumination [65]. Indeed, a substantial part of the NPQ generated in the *vde* KO mutants or the *psbs lhcsr* KO mutant did not relax after illumination (Supplementary Fig. 7). In *A. thaliana,* a slowly-rising component of the *npq1* mutant, unable to generate Zx, and the *npq4* mutant, lacking PsbS, was also linked to photodamage [29,41]. Another effect that could be observed as quenching is chloroplast movement. Red light induces photoprotective avoidance responses by chloroplasts in *P. patens* [45–47]. This movement decreases the chlorophyll fluorescence during the illumination period, which is observed as NPQ due to its effect on F'_m. Chloroplast movement can also impact the $(1\text{-qP})_{ss}$ value through the decrease of fluorescence.

The slowly-rising component is therefore most likely a combination of the NPQ dependent on Vx to Zx conversion, especially in the interaction with LhcSR, and to a smaller extent the avoidance responses by chloroplasts and photodamage, particularly when little photoprotective NPQ is generated. In absence of LhcSR, especially the more abundant LhcSR1, the amplitude of the slowly-rising component was severely reduced, indicating that LhcSR1 is the main protein driving the slowly-rising, Zx-dependent NPQ in *P. patens*. This highlights the critical role of LhcSR1, together with Zx, in facilitating effective photoprotection under high light.

4.2. The transient kinetic component

The second kinetic component necessary to describe NPQ induction is characterized by a transient peak in NPQ in all *P. patens* plants studied here except the *psbs lhcsr* KO. This component contains a transient NPQ peak that reaches its maximum after approximately one minute of illumination. The quick rise in NPQ provided by this kinetic component likely plays an important physiological role by providing rapid protection during short light exposures or fluctuating light conditions, especially when sustained photoprotection is not yet fully established. The relaxation of NPQ within a few minutes suggests that its fast induction is counteracted by processes that dissipate the proton gradient across the thylakoid membrane, especially at lower light intensities. Both PsbS [13] and LhcSR [18,20] are activated by the low luminal pH induced during illumination. As the pH difference across the thylakoid membrane contributes to the proton motive force that drives ATP synthesis, activation of the ATP synthase could decrease luminal acidification and thus reduce quenching. In addition, thylakoid-localized ion antiporters also modulate the pH difference and can influence NPQ [56,66,67] [56,66,67]. Together, these processes likely explain the relaxation of NPQ after its initial induction, resulting in a transient peak. Indeed, in *A. thaliana* two components with a transient peak were also associated with the rapid pH-dependent activation of PsbS [29,41]. Both PsbS and LhcSR induce a similar rise of NPQ in time, ensuring fast quenching of light energy (Fig. 4e). Vx to Zx conversion enhances LhcSR-dependent quenching of the transient kinetic component (Supplementary Fig. 13). Constitutive accumulation of Zx increases the initial quenching upon illumination, with a more pronounced effect for LhcSR-dependent quenching. Both PsbS and LhcSR are therefore able to independently generate fast protection necessary for natural, fluctuating light conditions. However, the PsbS-dependent contribution of this component is lower than the LhcSR-dependent contribution.

4.3. Comparison PsbS and LhcSR

Both PsbS and LhcSR seem to generate a similar transient profile in NPQ, providing rapid photoprotection. However, there are clear differences between these two NPQ trigger molecules. First, PsbS and LhcSR have different dependencies on Zx. The LhcSR-related NPQ in both components was heavily dependent on Vx to Zx conversion. Comparison of the *psbs KO* (able to convert Vx to Zx and with LhcSR) and *vde psbs KO* (not able to convert Vx to Zx and with LhcSR) shows that the ability to convert Vx to Zx induced amplifications of ~5- and ~ 4-fold for the LhcSR-dependent slowly-rising and transient component, respectively. The NPQ generated by LhcSR is enhanced by the conversion of Vx to Zx, at all light intensities and within a minute of illumination (Fig. 5). Because conversion of Vx to Zx proceeds on the several-minute timescale, only a small amount of Zx has formed after one minute [26], yet this limited amount of Zx or the difference in the de-epoxidation state of the xanthophyll pool [64] is sufficient to enhance

LhcSR-dependent quenching. That a limited amount of Zx is sufficient to drive NPQ has also been suggested for the seawater alga *Nannochloropsis oceanica*[68].

LhcSR has been shown to structurally interact with Zx [18,40], in contrast to PsbS which is not known to bind pigments [15,16]. A model based on *in vitro* studies on isolated LhcSR1 complexes suggested that LhcSR1 could adopt two distinct quenching states, one triggered by low luminal pH and the other by binding Zx [69]. A pH drop leads to a conformational change, which results in the quenched state [70]. In the *zep* KO, a pH-independent quenching state linked to LhcSR can occur in the dark, suggesting a quenching state dependent on Zx binding [43]. *In vivo*, the effect of quenching by LhcSR due to a drop in pH, without the presence of Zx, seems minimal compared to the quenching reached when able to interact with Zx (this study; [40]). *P. patens* LhcSR contains only four of the thirteen presumed protonatable residues found in LhcSR from *C. reinhardtii* [71]. Because protonatable residues are thought to play a key role in triggering conformational changes required for energy dissipation, this reduction could make *P. patens* LhcSR less responsive to lumen acidification alone. Consequently, *P. patens* LhcSR may rely more strongly on Zx binding to achieve efficient quenching, whereas NPQ in *C. reinhardtii* can proceed without Zx [18,37]. That accumulation of xanthophyll pigments is important for NPQ has been shown for proteins related to LhcSR as well. In the diatom *Phaeodactylum tricornutum*, NPQ has been shown to be proportional to the product of the concentration of Lhcx1, related to LhcSR proteins, and the proportion of the xanthophyll responsible for quenching (diatoxanthin) in the xanthophyll pool as a metric for the amount of Lhcx1 bound to diatoxanthin [33]. Determining the effect of different LhcSR concentrations and Zx accumulation on NPQ in *P. patens* would be interesting as well.

The nature of the interaction of PsbS and Zx remains unclear, as PsbS does not tightly bind pigments [15,16]. Comparison of the *lhcsr KO* (able to convert Vx to Zx and with PsbS) and *vde lhcsr KO* (not able to convert Vx to Zx and with PsbS) shows that Zx induced a slight amplification for the PsbS-dependent slowly-rising component. These differences are smaller than the Zx-induced differences observed in *A. thaliana* [29]. PsbS and Zx seem to amplify each other's quenching capacity, especially in vascular plants [29]. Second, while PsbS generally produces less NPQ, when grown under either high light or fluctuating light conditions, the production of PsbS increases more than the production of LhcSR [60,61]. This suggests that the regulation of PsbS production could be more in tune with environmental stressors [43].

5. Conclusion

NPQ in *P. patens* can be accurately described by two kinetic components. Our findings build on previous work demonstrating distinct NPQ components regulated by PsbS, LhcSR, and Zx [13,17,63]. The identification of two kinetic components with differential dependencies on these factors aligns with the multi-component NPQ models proposed in [8] and offers novel insights into the interplay of pigment-protein interactions. Fig. 6 shows a model that described NPQ in *P. patens*. A slowly-rising component (Fig. 6; left panel) provides most NPQ, especially at higher light intensities. Multiple processes contribute to this component. The highest contribution to this component stems from the NPQ that results from the interaction between LhcSR (especially the more abundant LhcSR1) and Zx. A smaller contribution originates from the functional interaction of PsbS and Zx. The slowly-rising component is still present in the mutants that generate limited photoprotective NPQ. In these mutants, the slowly-rising component is likely caused by photodamage-related NPQ and potentially avoidance responses by chloroplasts. Another kinetic component (Fig. 6; right panel) quickly rises and contains a transient peak in NPQ. Multiple processes contribute to this component as well. This component requires the presence of either PsbS or LhcSR. Both PsbS and LhcSR are therefore able to generate the rapid quenching necessary in fluctuating light conditions. The transient component dependent on LhcSR is enhanced if *P. patens* has the ability to convert Vx to Zx. The PsbS-related transient component generates less NPQ and is less dependent on Zx generation.

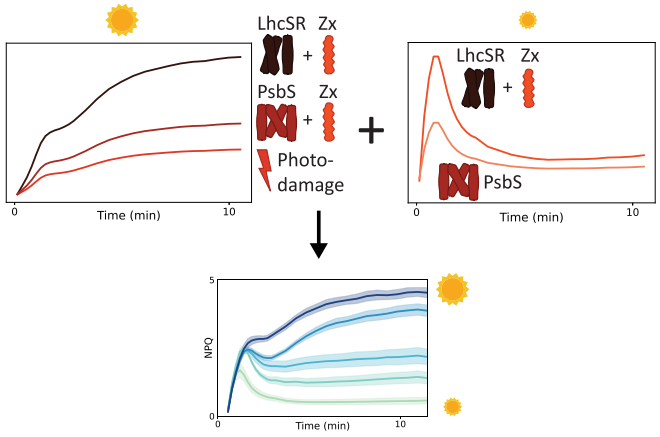

Fig. 6. Model to describe NPQ in *P. patens*. Two components are required to describe NPQ in *P. patens*. A slowly-rising component provides most NPQ, especially at higher light intensities. The highest contribution of the slowly-rising component occurs in plants that contain LhcSR and are able to convert Vx to Zx. PsbS also contributes to this component in a functional interaction with Zx. In mutants that generate little photoprotective NPQ, the slowly-rising component is likely caused by photodamage and potentially light avoidance responses of chloroplasts. The second kinetic component is more prominent at lower light intensities. It quickly rises and contains a transient peak in NPQ. This component requires the presence of either PsbS or LhcSR. Vx to Zx conversion enhances the LhcSR-dependent transient component. Together, these two components can describe NPQ at a range of light intensities in *P. patens*.

Our results corroborate and extend observations made in *P. patens* mutants in [40], emphasizing the central role of zeaxanthin in modulating LhcSR-dependent NPQ even at low light intensities. Furthermore, our data shows that Vx to Zx conversion plays a more extensive role in NPQ than previously appreciated, even at low light intensities and shortly after light exposure. The two distinct kinetic NPQ profiles are enhanced in plants that contain LhcSR and have the ability to convert Vx to Zx. The unexpected significance of Vx to Zx conversion in both transient and sustained NPQ components under low light challenges the traditional view of the xanthophyll cycle as being primarily a high-light response. This suggests that xanthophyll cycle-mediated modulation of NPQ begins earlier and may play a continuous role in photoprotection even during moderate fluctuating light conditions.

CRediT authorship contribution statement

Cleo Bagchus: Writing – original draft, Visualization, Investigation, Formal analysis, Data curation, Conceptualization. **Lennart A.I. Ramakers:** Writing – review & editing, Supervision, Formal analysis, Data curation, Conceptualization. **Dana Verhoeven:** Writing – review & editing, Visualization, Data curation. **Claudia Beraldo:** Writing – review & editing, Resources, Investigation. **Alessandro Alboresi:** Writing – review & editing, Supervision, Resources. **Tomas Morosinotto:** Writing – review & editing, Supervision, Resources, Conceptualization. **Herbert van Amerongen:** Writing – review & editing, Supervision, Project administration, Funding acquisition, Conceptualization. **Emilie Wientjes:** Writing – review & editing, Supervision, Project administration, Funding acquisition, Conceptualization.

Declaration of competing interest

The authors declare the following financial interests/personal relationships which may be considered as potential competing interests: Emilie Wientjes reports financial support was provided by Dutch Research Council. Herbert van Amerongen reports financial support was

provided by Dutch Research Council. If there are other authors, they declare that they have no known competing financial interests or personal relationships that could have appeared to influence the work reported in this paper.

Acknowledgements

The authors would like to acknowledge NWO for funding this research project 'Nanoscale regulators of photosynthesis' (project number: OCENW.GROOT.2019.86). The authors would like to thank the Laboratory of Biochemistry at Wageningen University for the use of their plant growth facilities.

Appendix A. Supplementary data

Supplementary data to this article can be found online at https://doi.org/10.1016/j.bbabio.2026.149581.

Data availability

Data will be made available on the data repository 4TU with doi 10.4121/5417e149-4c9c-4a44-8424-bfd4a8ecdd07

References

[1] K. Asada, Production and scavenging of reactive oxygen species in chloroplasts and their functions, in: Plant Physiology Vol. 141, Issue 2, American Society of Plant Biologists, 2006, pp. 391–396, https://doi.org/10.1104/pp.106.082040.
[2] A. Telfer, Singlet oxygen production by PSII under light stress: mechanism, detection and the protective role of β-carotene, in: Plant and Cell Physiology Vol. 55, Issue 7, Oxford University Press, 2014, pp. 1216–1223, https://doi.org/10.1093/pcp/pcu040.
[3] I. Vass, Role of charge recombination processes in photodamage and photoprotection of the photosystem II complex, Physiol. Plant. 142 (1) (2011) 6–16, https://doi.org/10.1111/j.1399-3054.2011.01454.x.
[4] J.D. Rochaix, Regulation and dynamics of the light-harvesting system, Annual Review of Plant Biology 65 (2014) 287–309. Annual Reviews Inc, https://doi.org/10.1146/annurev-arplant-050213-040226.
[5] B. Demmig-Adams, C.M. Cohu, O. Muller, W.W. Adams, Modulation of photosynthetic energy conversion efficiency in nature: from seconds to seasons, Photosynth. Res. 113 (1–3) (2012) 75–88, https://doi.org/10.1007/s11120-012-9761-6.
[6] P. Horton, A.V. Ruban, R.G. Walters, Regulation of light harvesting in green plants, in: Annu. Rev. Plant Physiol. Plant Mol. Biol Vol. 47), 1996.
[7] K.K. Niyogi, T.B. Truong, Evolution of flexible non-photochemical quenching mechanisms that regulate light harvesting in oxygenic photosynthesis, Current Opinion in Plant Biology 16 (3) (2013) 307–314, https://doi.org/10.1016/j.pbi.2013.03.011.
[8] A.V. Ruban, M.P. Johnson, C.D.P. Duffy, The photoprotective molecular switch in the photosystem II antenna, Biochimica et Biophysica Acta - bioenergetics 1817 (1) (2012) 167–181, https://doi.org/10.1016/j.bbabio.2011.04.007.
[9] H. van Amerongen, R. Croce, Non-photochemical quenching in plants: mechanisms and mysteries, Plant Cell koaf240 (2025), https://doi.org/10.1093/plcell/koaf240.
[10] A.P. De Souza, S.J. Burgess, L. Doran, J. Hansen, L. Manukyan, N. Maryn, D. Gotarkar, L. Leonelli, K.K. Niyogi, S.P. Long, Soybean photosynthesis and crop yield are improved by accelerating recovery from photoprotection, Plant Sci. 377 (2022) 851–854. https://www.science.org.
[11] J. Kromdijk, K. Glowacka, L. Leonelli, S.T. Gabilly, M. Iwai, K.K. Niyogi, S.P. Long, Improving photosynthesis andcrop productivity by acceleratingrecovery from photoprotection, Science 354 (6314) (2016) 851–857, https://doi.org/10.1126/science.aaf9621.
[12] X.G. Zhu, S.P. Long, D.R. Ort, Improving photosynthetic efficiency for greater yield, Annu. Rev. Plant Biol. 61 (2010) 235–261, https://doi.org/10.1146/annurev-arplant-042809-112206.
[13] X.-P. Li, O. Bjo, È. Rkman, C. Shih, A.R. Grossman, M. Rosenquist, S. Jansson, K. K. Niyogi, A pigment-binding protein essential for regulation of photosynthetic light harvesting, Nature 403 (2000). www.nature.com.
[14] W. Marulanda Valencia, A. Pandit, Photosystem II subunit S (PsbS): a nano regulator of plant photosynthesis, Journal of Molecular Biology 436 (5) (2024), https://doi.org/10.1016/j.jmb.2023.168407. Academic Press.
[15] P. Dominici, S. Caffarri, F. Armenante, S. Ceoldo, M. Crimi, R. Bassi, Biochemical properties of the PsbS subunit of photosystem II either purified from chloroplast or recombinant, J. Biol. Chem. 277 (25) (2002) 22750–22758, https://doi.org/10.1074/jbc.M200604200.
[16] M. Fan, M. Li, Z. Liu, P. Cao, X. Pan, H. Zhang, X. Zhao, J. Zhang, W. Chang, Crystal structures of the PsbS protein essential for photoprotection in plants, Nat. Struct. Mol. Biol. 22 (9) (2015) 729–735, https://doi.org/10.1038/nsmb.3068.
[17] G. Peers, T.B. Truong, E. Ostendorf, A. Busch, D. Elrad, A.R. Grossman, M. Hippler, K.K. Niyogi, An ancient light-harvesting protein is critical for the regulation of algal photosynthesis, Nature 462 (7272) (2009) 518–521, https://doi.org/10.1038/nature08587.
[18] G. Bonente, M. Ballottari, T.B. Truong, T. Morosinotto, T.K. Ahn, G.R. Fleming, K. K. Niyogi, R. Bassi, Analysis of LHcSR3, a protein essential for feedback de-excitation in the green alga Chlamydomonas reinhardtii, PLoS Biol. 9 (1) (2011), https://doi.org/10.1371/journal.pbio.1000577.
[19] K.K. Niyogi, T.B. Truong, Evolution of flexible non-photochemical quenching mechanisms that regulate light harvesting in oxygenic photosynthesis, Current Opinion in Plant Biology 16 (3) (2013) 307–314, https://doi.org/10.1016/j.pbi.2013.03.011.
[20] N. Liguori, L.M. Roy, M. Opacic, G. Durand, R. Croce, Regulation of light harvesting in the green alga chlamydomonas reinhardtii: the c-terminus of lhcsr is the knob of a dimmer switch, J. Am. Chem. Soc. 135 (49) (2013) 18339–18342, https://doi.org/10.1021/ja4107463.
[21] P. Arnoux, T. Morosinotto, G. Saga, R. Bassi, D. Pignol, A structural basis for the ph-dependent xanthophyll cycle in arabidopsis thaliana, Plant Cell 21 (7) (2009) 2036–2044, https://doi.org/10.1105/tpc.109.068007.
[22] B. Demmig, K. Winter, A. Krüger, F.-C. Czygan, Photoinhibition and Zeaxanthin Formation in Intact Leaves: A Possible Role of the Xanthophyll Cycle in the Dissipation of Excess Light Energy. In Source: Plant Physiology Vol. 84, Issue 2, 1987. https://about.jstor.org/terms.
[23] H.Y. Yamamoto, M. Nakayama, C.O. Chichester, Studies on the light and dark interconversions of leaf Xanthophylls, Arch. Biochem. Biophys. 97 (1962) 168–173.
[24] R.C. Bugos, A.D. Hieber, H.Y. Yamamoto, Xanthophyll cycle enzymes are members of the lipocalin family, the first identified from plants, J. Biol. Chem. 273 (25) (1998) 15321–15324, https://doi.org/10.1074/jbc.273.25.15321.
[25] E. Kress, P. Jahns, The dynamics of energy dissipation and xanthophyll conversion in arabidopsis indicate an indirect photoprotective role of zeaxanthin in slowly inducible and relaxing components of non-photochemical quenching of excitation energy, Front. Plant Sci. 8 (2017), https://doi.org/10.3389/fpls.2017.02094.
[26] L. Küster, R. Lücke, C. Brabender, S. Bethmann, P. Jahns, The amount of zeaxanthin epoxidase but not the amount of Violaxanthin De-epoxidase is a critical determinant of zeaxanthin accumulation in Arabidopsis thaliana and Nicotiana tabacum, Plant Cell Physiol. 64 (10) (2023) 1220–1230, https://doi.org/10.1093/pcp/pcad091.
[27] C. Reinhold, S. Niczyporuk, K.C. Beran, P. Jahns, Short-term down-regulation of zeaxanthin epoxidation in Arabidopsis thaliana in response to photo-oxidative stress conditions, Biochimica et Biophysica Acta - Bioenergetics 1777 (5) (2008) 462–469, https://doi.org/10.1016/j.bbabio.2008.03.002.
[28] X.-P. Li, P. Mü Ller-Moulé, A.M. Gilmore, K.K. Niyogi, PsbS-dependent enhancement of feedback de-excitation protects photosystem II from photoinhibition, PNAS 99 (23) (2002) 15222–15227. www.pnas.orgcgidoi10.1073pnas.232447699.
[29] L.A.I. Ramakers, J. Harbinson, H. van Amerongen, A novel multivariate analysis: overturning long-held beliefs about non-photochemical quenching, Physiol. Plant. 177 (4) (2025), https://doi.org/10.1111/ppl.70420.
[30] V. Mascoli, N. Liguori, P. Xu, L.M. Roy, I.H.M. van Stokkum, R. Croce, Capturing the quenching mechanism of light-harvesting complexes of plants by zooming in on the ensemble, Chem 5 (11) (2019) 2900–2912, https://doi.org/10.1016/j.chempr.2019.08.002.
[31] B. Van Oort, A. Van Hoek, A.V. Ruban, H. Van Amerongen, Equilibrium between quenched and nonquenched conformations of the major plant light-harvesting complex studied with high-pressure time-resolved fluorescence, J. Phys. Chem. B 111 (26) (2007) 7631–7637, https://doi.org/10.1021/jp070573z.
[32] B. Bailleul, A. Rogato, A. De Martino, S. Coesel, P. Cardol, C. Bowler, A. Falciatore, G. Finazzi, An atypical member of the light-harvesting complex stress-related protein family modulates diatom responses to light, Proc. Natl. Acad. Sci. U. S. A. 107 (42) (2010) 18214–18219, https://doi.org/10.1073/pnas.1007703107.
[33] D. Croteau, M. Jaubert, A. Falciatore, B. Bailleul, Pennate diatoms make non-photochemical quenching as simple as possible but not simpler, Nature Communications 16 (1) (2025), https://doi.org/10.1038/s41467-025-57298-4.
[34] S.H. Zhu, B.R. Green, Photoprotection in the diatom Thalassiosira pseudonana: role of LI818-like proteins in response to high light stress, Biochim. Biophys. Acta Bioenerg. 1797 (8) (2010) 1449–1457, https://doi.org/10.1016/j.bbabio.2010.04.003.
[35] S.M. Dittami, G. Michel, J. Collén, C. Boyen, T. Tonon, Chlorophyll-binding proteins revisited - a multigenic family of light-harvesting and stress proteins from a brown algal perspective, BMC Evol. Biol. 10 (1) (2010), https://doi.org/10.1186/1471-2148-10-365.
[36] A. Alboresi, C. Gerotto, G.M. Giacometti, R. Bassi, T. Morosinotto, Physcomitrella patens mutants affected on heat dissipation clarify the evolution of photoprotection mechanisms upon land colonization, Proc. Natl. Acad. Sci. U. S. A. 107 (24) (2010) 11128–11133, https://doi.org/10.1073/pnas.1002873107.
[37] A. Pinnola, The rise and fall of light-harvesting complex stress-related proteins as photoprotection agents during evolution, J. Exp. Bot. 70 (20) (2019) 5527–5535, https://doi.org/10.1093/jxb/erz317.
[38] A. Alboresi, S. Caffarri, F. Nogue, R. Bassi, T. Morosinotto, In silico and biochemical analysis of Physcomitrella patens photosynthetic antenna: identification of subunits which evolved upon land adaptation, PloS One 3 (4) (2008), https://doi.org/10.1371/journal.pone.0002033.
[39] C. Gerotto, A. Alboresi, G.M. Giacometti, R. Bassi, T. Morosinotto, Coexistence of plant and algal energy dissipation mechanisms in the moss Physcomitrella patens,

New Phytol. 196 (3) (2012) 763–773, https://doi.org/10.1111/j.1469-8137.2012.04345.x.
[40] A. Pinnola, L. Dall'Osto, C. Gerotto, T. Morosinotto, R. Bassi, A. Alboresi, Zeaxanthin binds to light-harvesting complex stress-related protein to enhance nonphotochemical quenching in Physcomitrella patens, Plant Cell 25 (9) (2013) 3519–3534, https://doi.org/10.1105/tpc.113.114538.
[41] L.A.I. Ramakers, J. Harbinson, E. Wientjes, H. van Amerongen, Unravelling the different components of nonphotochemical quenching using a novel analytical pipeline, New Phytol. 245 (2025) 625–636, https://doi.org/10.1111/nph.20271.
[42] D. Takezawa, N. Watanabe, T.K. Ghosh, M. Saruhashi, A. Suzuki, K. Ishiyama, S. Somemiya, M. Kobayashi, Y. Sakata, Epoxycarotenoid-mediated synthesis of abscisic acid in Physcomitrella patens implicating conserved mechanisms for acclimation to hyperosmosis in embryophytes, New Phytol. 206 (1) (2015) 209–219, https://doi.org/10.1111/nph.13231.
[43] C. Beraldo, C. Bagchus, D. Verhoeven, A. Bellan, C. Gerotto, E. Wientjes, H. Amerongen van, T. Morosinotto, A. Alboresi, Functional divergence of LHCSR and PSBS in zeaxanthin-mediated non-photochemical quenching, Research Square [PREPRINT], 2025.
[44] N.W. Ashton, N.H. Grimsley, D.J. Cove, Analysis of Gametophytie development in the Moss, Physcomitrella patens, using auxin and cytokinin resistant mutants, in: Planta 144, 1979.
[45] A. Kadota, Y. Sato, M. Wada, Intracellular chloroplast photorelocation in the moss Physcomitrella patens is mediated by phytochrome as well as by a blue-light receptor, Planta 210 (2000) 932–937.
[46] M. Kasahara, T. Kagawa, Y. Sato, T. Kiyosue, M. Wada, Phototropins mediate blue and red light-induced chloroplast movements in Physcomitrella patens, Plant Physiol. 135 (3) (2004) 1388–1397, https://doi.org/10.1104/pp.104.042705.
[47] Y. Sato, M. Wada, A. Kadota, Choice of tracks, microtubules and/or actin filaments for chloroplast photo-movement is differentially controlled by phytochrome and a blue light receptor, J. Cell Sci. 114 (2) (2001).
[48] R. Fritzsch, P.M. Donaldson, G.M. Greetham, M. Towrie, A.W. Parker, M.J. Baker, N.T. Hunt, Rapid screening of DNA-ligand complexes via 2D-IR spectroscopy and ANOVA-PCA, Anal. Chem. 90 (4) (2018) 2732–2740, https://doi.org/10.1021/acs.analchem.7b04727.
[49] A. Mackiewicz, W. Ratajczak, Principal components analysis (PCA), Comput. Geosci. 19 (3) (1993) 303.
[50] D.A. Jackson, Stopping rules in Principal components analysis: a comparison of Heuristical and statistical approaches, Ecology 74 (8) (1993) 2204–2214.
[51] A. Bader, N. Visser, H. van Amerongen, A. Visser, Phasor approaches simplify the analysis of tryptophan fluorescence data in protein denaturation studies, Methods and Applications in Fluorescence 2 (2014) 4.
[52] W.M.J. Franssen, F.J. Vergeldt, A.N. Bader, H. Van Amerongen, C. Terenzi, Full-harmonics phasor analysis: unravelling multiexponential trends in magnetic resonance imaging data, J. Phys. Chem. Lett. 11 (21) (2020) 9152–9158, https://doi.org/10.1021/acs.jpclett.0c02319.
[53] O. Pârvu, D. Gilbert, Implementation of linear minimum area enclosing triangle algorithm: application note, Comput. Appl. Math. 35 (2) (2016) 423–438, https://doi.org/10.1007/s40314-014-0198-8.
[54] B. Torrado, L. Malacrida, S. Ranjit, Linear combination properties of the phasor space in fluorescence imaging, Sensors 22 (3) (2022), https://doi.org/10.3390/s22030999. MDPI.
[55] M.W. Berry, M. Browne, A.N. Langville, V.P. Pauca, R.J. Plemmons, Algorithms and applications for approximate nonnegative matrix factorization, Computational Statistics and Data Analysis 52 (1) (2007) 155–173, https://doi.org/10.1016/j.csda.2006.11.006.
[56] U. Armbruster, L. Leonelli, V.C. Galvis, D. Strand, E.H. Quinn, M.C. Jonikas, K. K. Niyogi, Regulation and levels of the thylakoid K+/H+ antiporter KEA3 shape the dynamic response of photosynthesis in fluctuating light, Plant and Cell Physiology 57 (7) (2016) 1557–1567, https://doi.org/10.1093/pcp/pcw085.
[57] P. Horton, A.V. Ruban, M. Wentworth, Allosteric regulation of the light-harvesting system of photosystem II, Philos. Trans. R. Soc., B 355 (1402) (2000) 1361–1370, https://doi.org/10.1098/rstb.2000.0698.
[58] C. Neubauer, Multiple effects of Dithiothreitol on nonphotochemical fluorescence quenching in lntact chloroplasts' lnfluence on Violaxanthin De-epoxidase and ascorbate peroxidase activity, Plant Physiol 103 (1993). https://academic.oup.com/plphys/article/103/2/575/6067795.
[59] S.A. Rensing, B. Goffinet, R. Meyberg, S.Z. Wu, M. Bezanilla, The moss physcomitrium (Physcomitrella) patens: A model organism for non-seed plants, in: Plant Cell Vol. 32, Issue 5, American Society of Plant Biologists, 2020, pp. 1361–1376, https://doi.org/10.1105/tpc.19.00828.
[60] C. Beraldo, C. Toffanin, T. Morosinotto, A. Alboresi, Additive effects of multiple photoprotective mechanisms drive efficient photosynthesis under variable light conditions, Plant, Cell Environ. (2025), https://doi.org/10.1111/pce.70016.
[61] C. Gerotto, A. Alboresi, G.M. Giacometti, R. Bassi, T. Morosinotto, Role of PSBS and LHCSR in Physcomitrella patens acclimation to high light and low temperature, Plant, Cell Environ. 34 (6) (2011) 922–932, https://doi.org/10.1111/j.1365-3040.2011.02294.x.
[62] M.P. Johnson, M.L. Pérez-Bueno, A. Zia, P. Horton, A.V. Ruban, The zeaxanthin-independent and zeaxanthin-dependent qE components of nonphotochemical quenching involve common conformational changes within the photosystem II antenna in Arabidopsis, Plant Physiol. 149 (2) (2009) 1061–1075, https://doi.org/10.1104/pp.108.129957.
[63] M. Nilkens, E. Kress, P. Lambrev, Y. Miloslavina, M. Müller, A.R. Holzwarth, P. Jahns, Identification of a slowly inducible zeaxanthin-dependent component of non-photochemical quenching of chlorophyll fluorescence generated under steady-state conditions in Arabidopsis, Biochimica et Biophysica Acta - Bioenergetics 1797 (4) (2010) 466–475, https://doi.org/10.1016/j.bbabio.2010.01.001.
[64] M.P. Johnson, P.A. Davison, A.V. Ruban, P. Horton, The xanthophyll cycle pool size controls the kinetics of non-photochemical quenching in Arabidopsis thaliana, FEBS Lett. 582 (2) (2008) 262–266, https://doi.org/10.1016/j.febslet.2007.12.016.
[65] E. Tyystjarvi, E.-M. Aro, The rate constant of photoinhibition, measured in lincomycin-treated leaves, is directly proportional to light intensity, Plant Biology 93 (1996). https://www.pnas.org.
[66] U. Armbruster, L.R. Carrillo, K. Venema, L. Pavlovic, E. Schmidtmann, A. Kornfeld, P. Jahns, J.A. Berry, D.M. Kramer, M.C. Jonikas, Ion antiport accelerates photosynthetic acclimation in fluctuating light environments, Nat. Commun. 5 (2014), https://doi.org/10.1038/ncomms6439.
[67] C. Yanez-Dominguez, K. Macedo-Osorio, D. Lagunas-Gomez, D. Torres-Cifuentes, J. Castillo-Gonzalez, G. Zavala, O. Pantoja, The chloroplast-located HKT transporter plays an important role in fertilization and development in Physcomitrium patens, Plant J. 121 (3) (2025), https://doi.org/10.1111/tpj.17253.
[68] T. Michelberger, E. Mezzadrelli, A. Bellan, G. Perin, T. Morosinotto, The xanthophyll cycle balances photoprotection and photosynthetic efficiency in the seawater alga Nannochloropsis oceanica, Plant Physiol. 198 (3) (2025), https://doi.org/10.1093/plphys/kiaf301.
[69] T. Kondo, A. Pinnola, W.J. Chen, L. Dall'Osto, R. Bassi, G.S. Schlau-Cohen, Single-molecule spectroscopy of LHCSR1 protein dynamics identifies two distinct states responsible for multi-timescale photosynthetic photoprotection, Nat. Chem. 9 (8) (2017) 772–778, https://doi.org/10.1038/NCHEM.2818.
[70] L. Pedraza-González, E. Cignoni, J. D'Ascenzi, L. Cupellini, B. Mennucci, How the pH controls photoprotection in the light-harvesting complex of mosses, J. Am. Chem. Soc. 145 (13) (2023) 7482–7494, https://doi.org/10.1021/jacs.3c00377.
[71] M. Ballottari, T.B. Truong, E. Re De, E. Erickson, G.R. Stella, G.R. Fleming, R. Bassi, K.K. Niyogi, Identification of ph-sensing sites in the light harvesting complex stress-related 3 protein essential for triggering non-photochemical quenching in chlamydomonas reinhardtii, J. Biol. Chem. 291 (14) (2016) 7334–7346, https://doi.org/10.1074/jbc.M115.704601.